Supplementary Figure S1

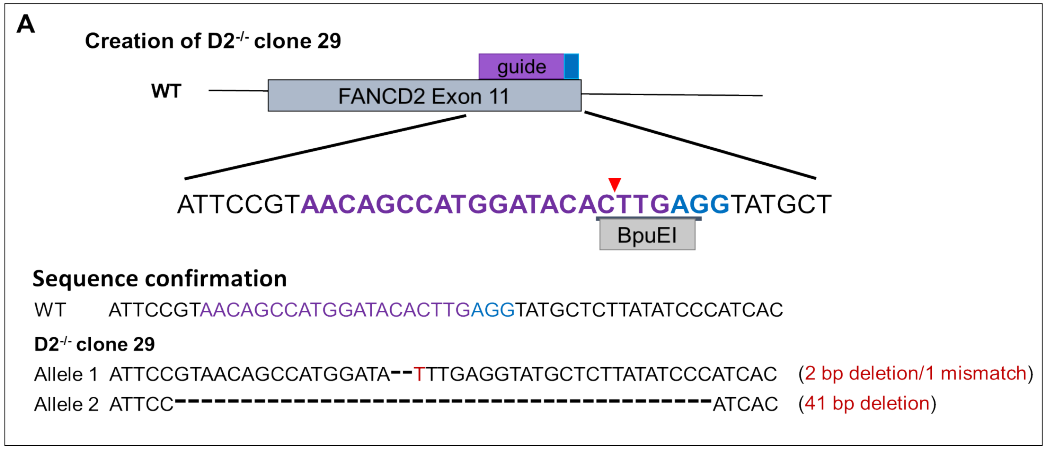

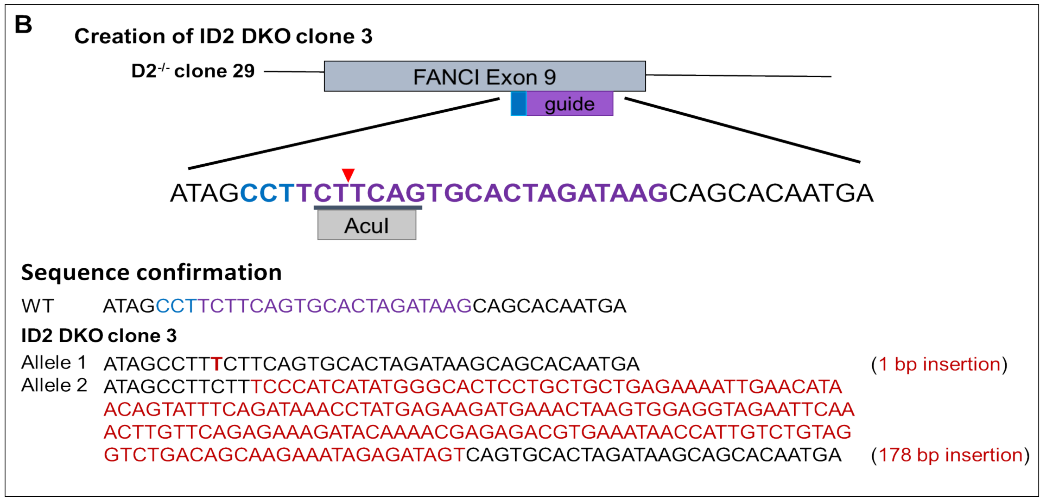

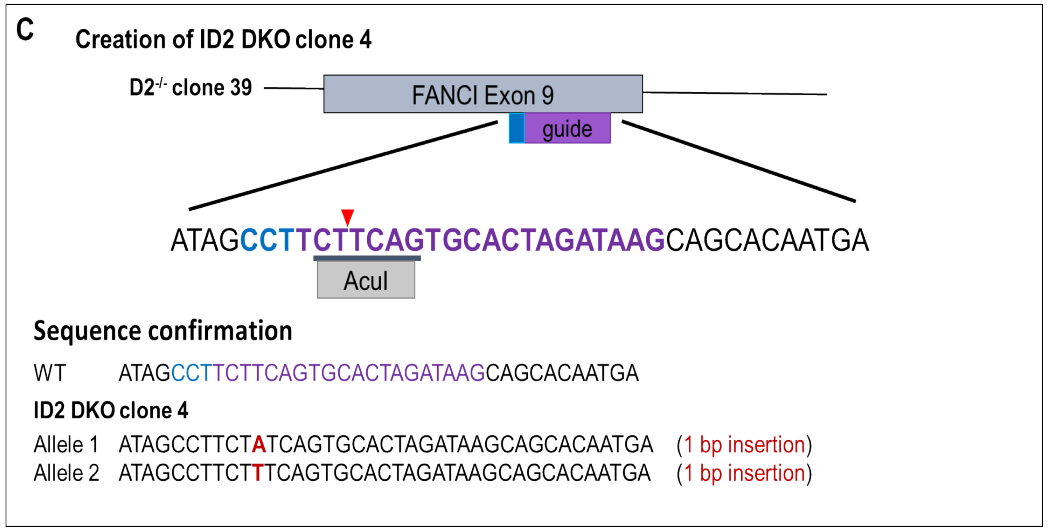

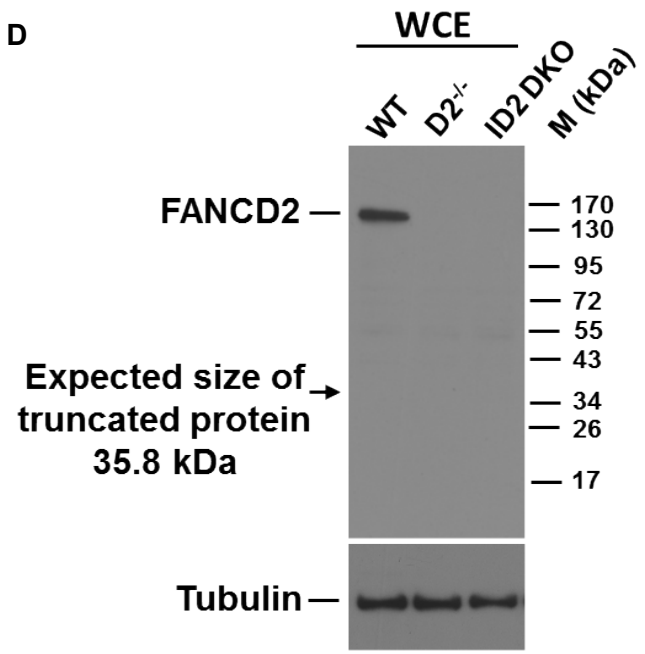

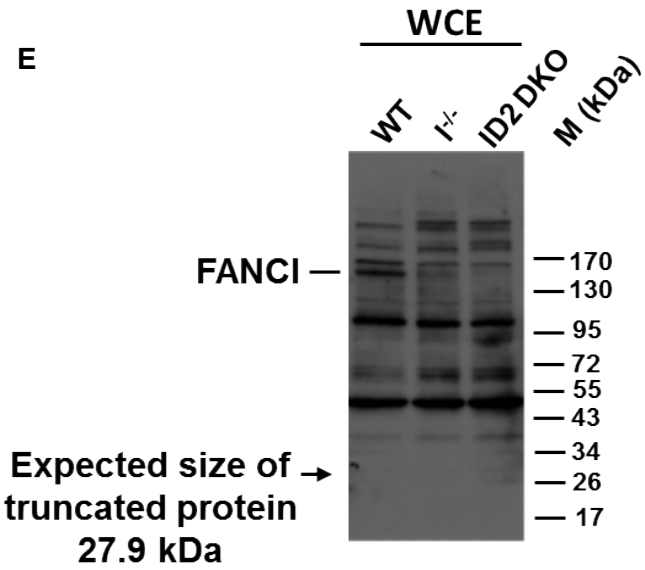

Supplementary Figure S2

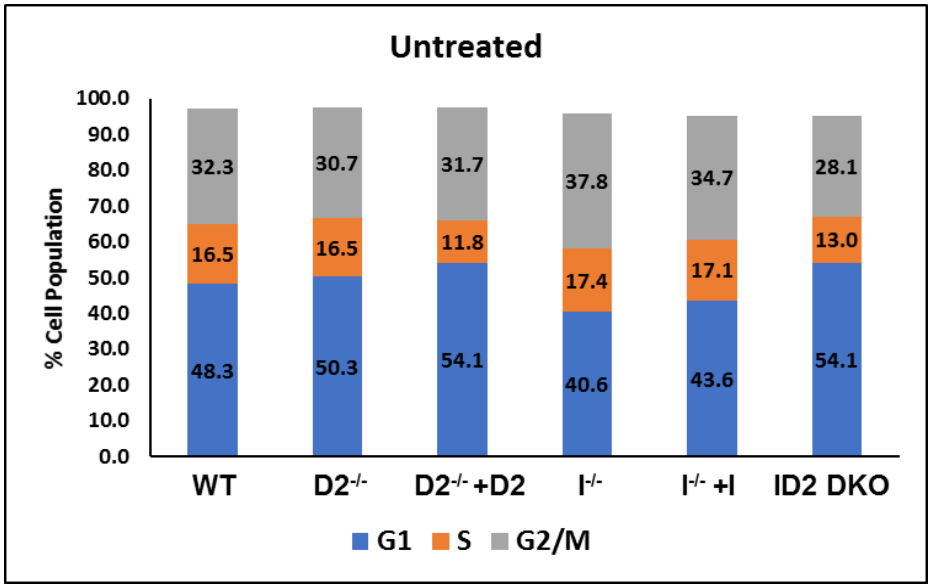

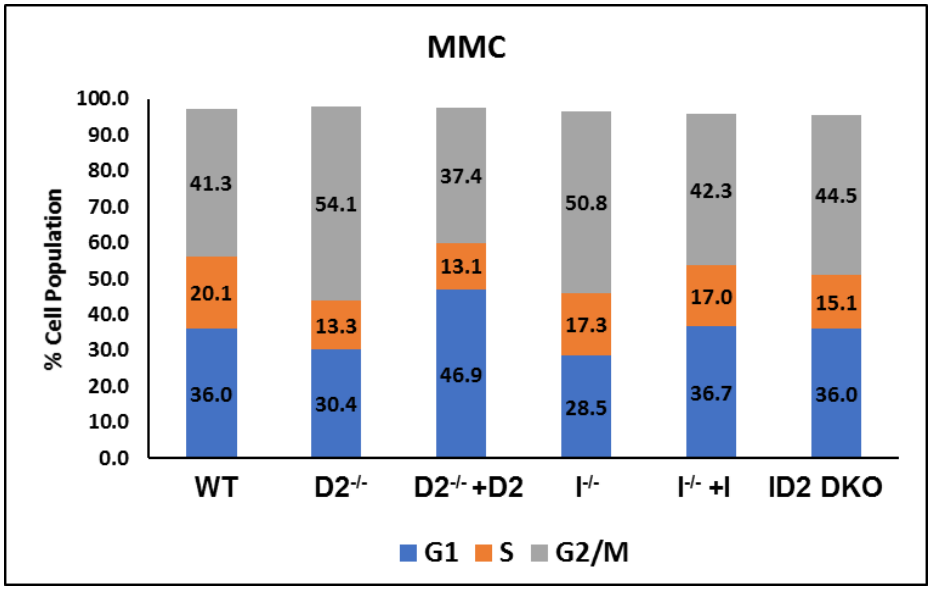

Supplementary Figure S3

A

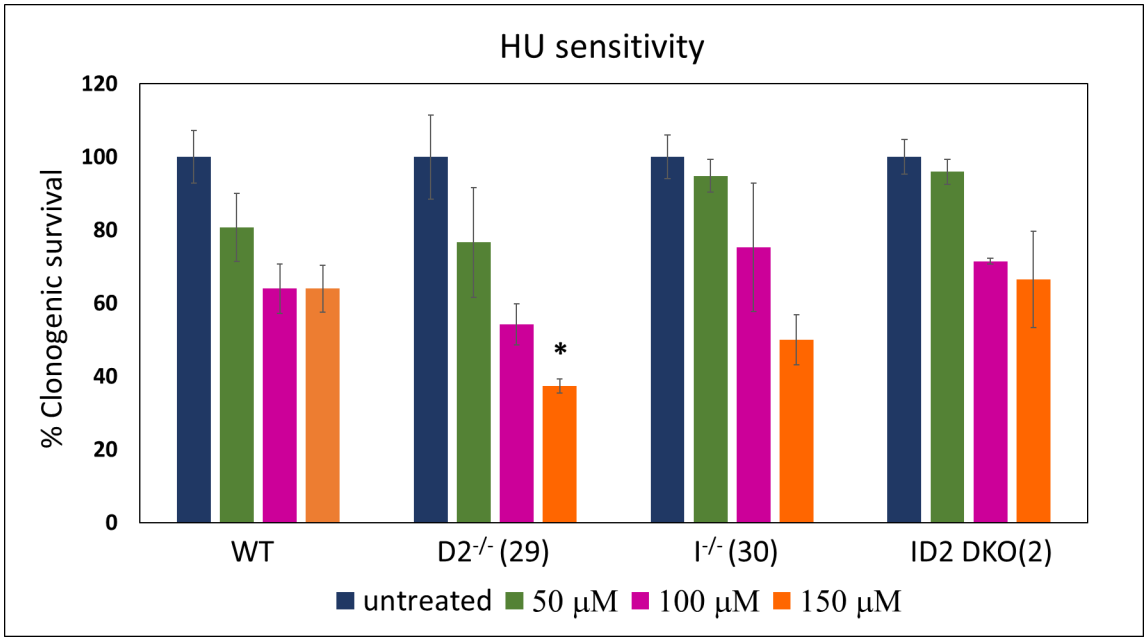

B

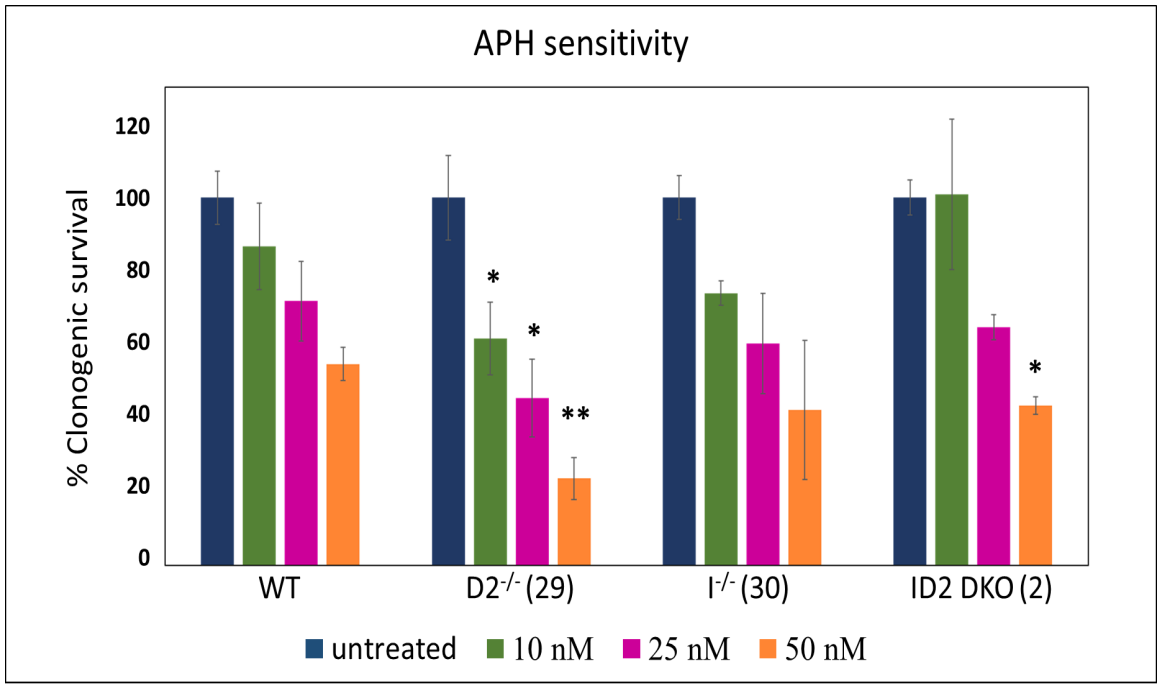

Supplementary Figure S4

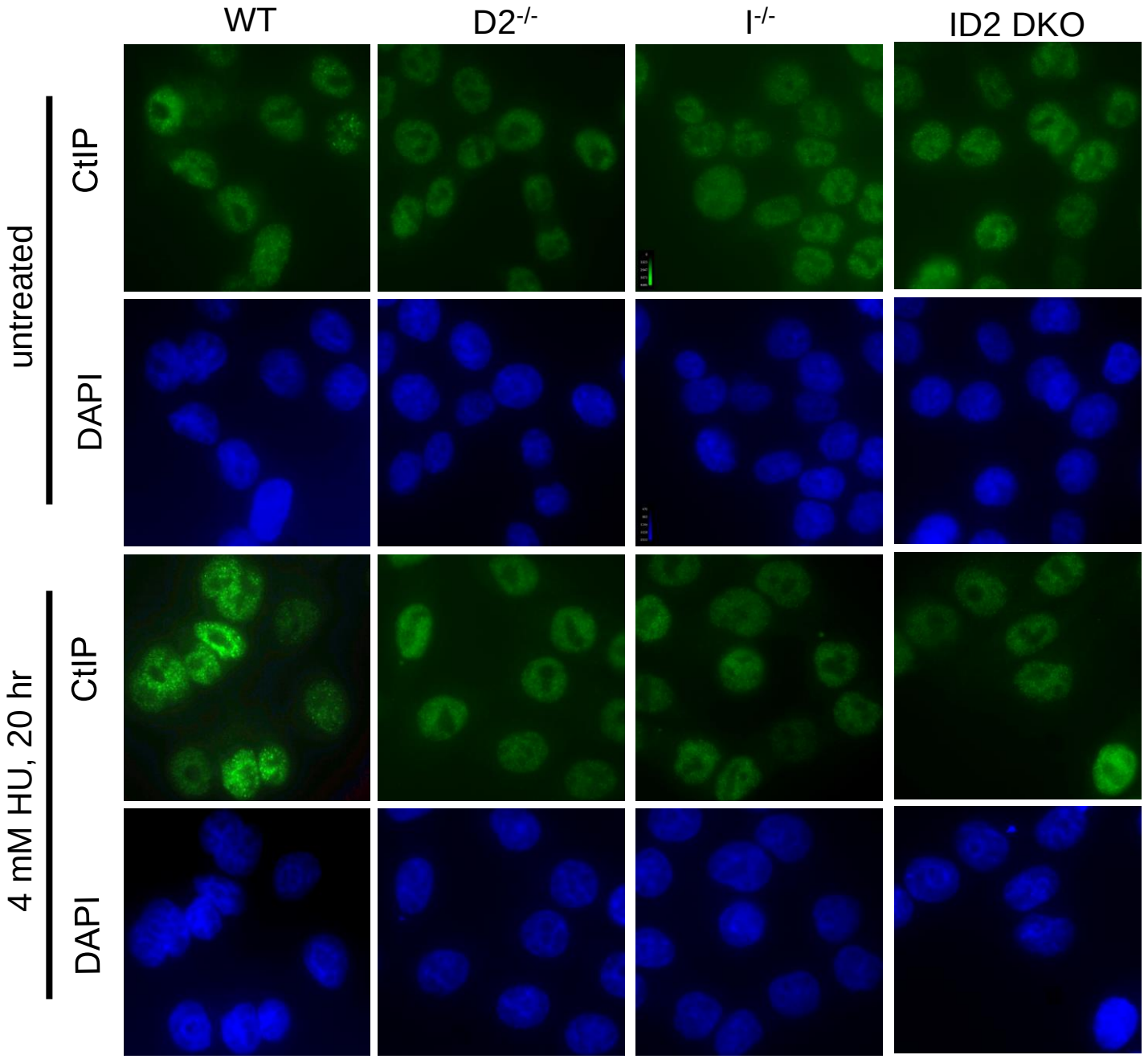

Supplementary Figure S5

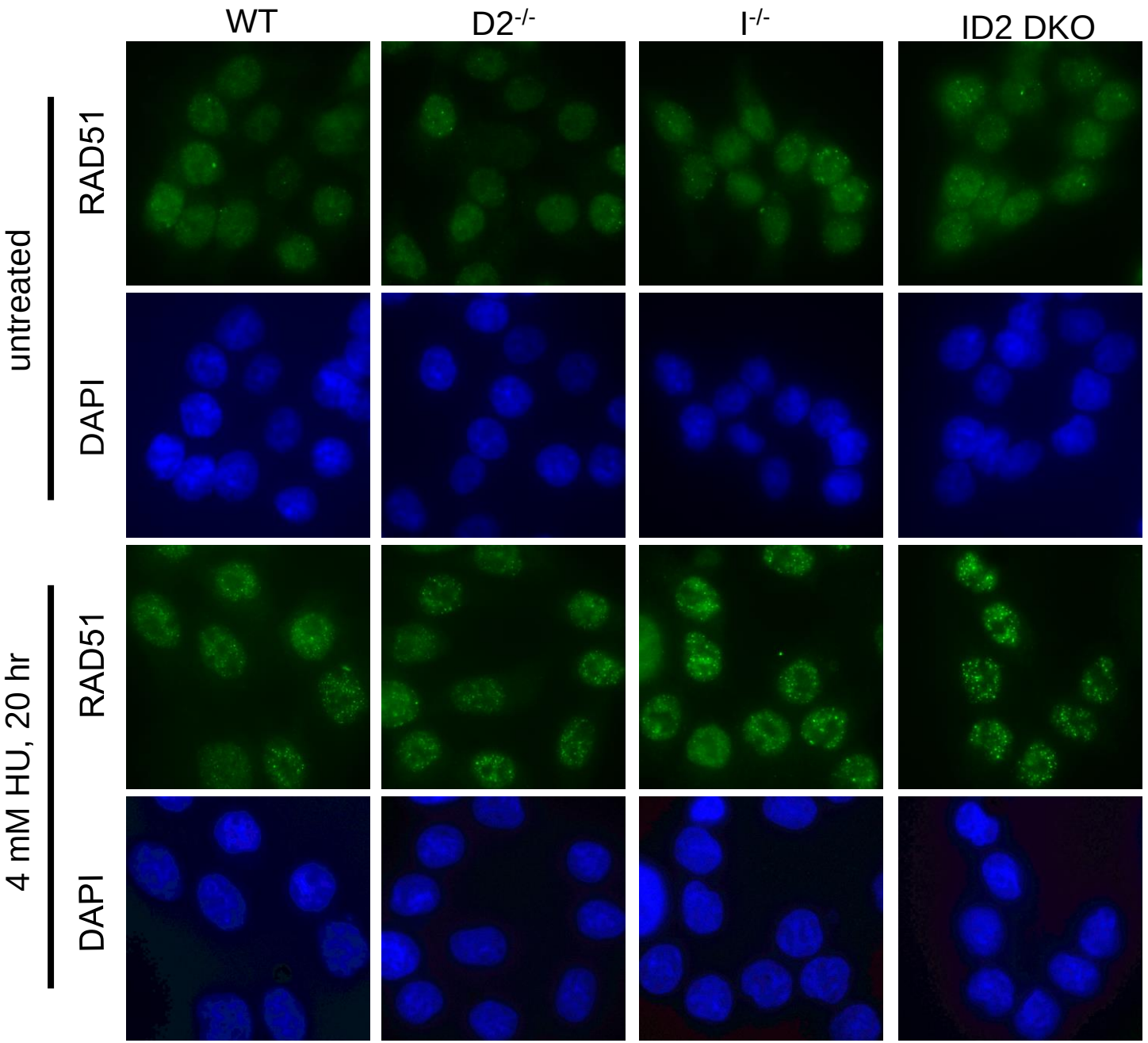

Supplementary Figure S6

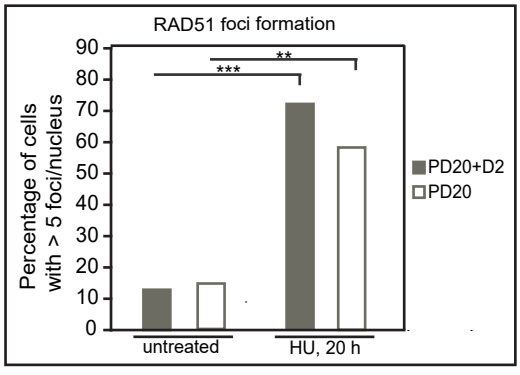

Supplementary Figure S7

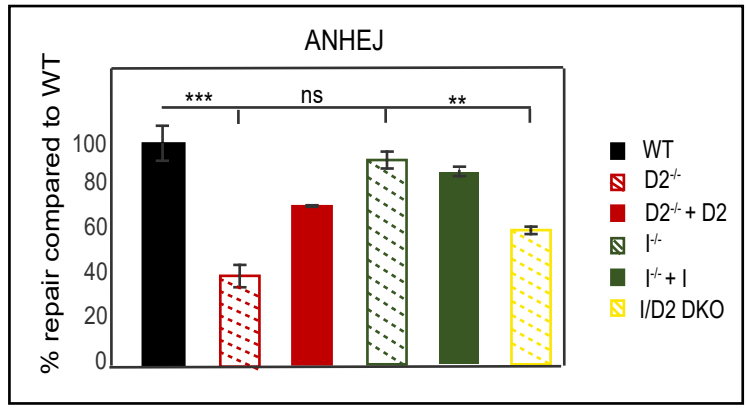

Supplementary Table S1

Primers

FANCD2 rAAV Conditional Vector Targeting Exon 12: Golden Gate Cloning primers

hFANCD2_LF_GG	GACGCTCTTCACCGTGACCCAAACTTCCTATTGA
hFANCD2_LR_GG	GACGCTCTTCTGAGGTTGCTTTATCTAGGTGTGA
hFANCD2_RF_GG	GACGCTCTTCGGCACAGACTAACTGAGAATACTGAC
hFANCD2_IR_GG	GACGCTCTTCGGTATGCTATACGAAGTTATGGATTGATCTGAATGGCTAAG
hFANCD2_IF_GG	GACGCTCTTCCTACATTATACGAAGTTATCAGACGACAGTGCAAGTT
hFANCD2_RR_GG	GACGCTCTTCCCGCCGCCACCTCAGATTATCTT

FANCD2 rAAV Knockout Vector Targeting Exon 12: Golden Gate Cloning primers

FANCD2-St KO-LF	GACGCTCTTCACCG GTGACCTACTGATAGAGAATAC
FANCD2-St KO-LR	GACGCTCTTCTGAG TAAGAGCATACCTCAAGTGT
FANCD2-ST KO-RF	GACGCTCTTCGTCAAAGAGCTCATCCTCACAC
FANCD2-ST KO-RR	GACGCTCTTCCATGTTGACAGTGGACAGATTGA

FANCD2 Allele Determination rAAV Targeting

FANCD2_EX11SF	ATTCTTCATTCCGTAACAGC
FANCD2_LoxP SR	GACAACCTCATGTATAAGATGG

FANCI rAAV Conditional Vector Targeting Exon 10: Golden Gate Cloning primers

FancI_GG_LF	GACGCTCTTCACCGGCTCAGGAGTTCAAGACC
FancI_GG_LR	GACGCTCTTCTGAGTCAAGACCAGCCTCTACTAA
FancIcond_GG_RF	GACGCTCTTCGTCACTCCTGGGATCAAGTGAT
FancIcond_GG_IR	GACGCTCTTCGGTATGCTATACGAAGTTATGAGTGTGGTAACATCATGTA
FancIcond_GG_IF	GACGCTCTTCCTACATTATACGAAGTTATTAATGTCCTCACTTTAGCAG
FancIcond_GG_RR	GACGCTCTTCCATGGAACAACCAAATGCAATGC

FANCI Allele Determination rAAV Targeting

FancIc_GG_LIF	GCAATGGCACAATCTTGG
FancIcond_GG_LoxR	ATAGGACTTTCTGGCTTGCT

CRISPR/Cas9 Targeting of FANCD2 Exon 11

FANCD2 gRNA sequence	AACAGCCATGGATACACTTG
FancD2_CC_ F2	GGAAGATGGAGTAAGAGAAGT
FancD2_CC_ R2	TGCTCATTCATAGTGGGTAG

CRISPR/Cas9 Targeting of FANCI Exon 9

FANCI gRNA sequence	CTTATCTAGTGCACTGAAGA
FancI_CC _F3	TTCTCTGCTCCCAAGTTTC
FancI_CC _R3	TGTGCTGAGGTGAAGGTA

Supplementary Table S2

Figure	samples	p-value (two tales)
4A	$D2^{-/-}$ vs $I^{-/-}$	0.033561
	$D2^{-/-}$ vs ID2 DKO	0.0000029
	$I^{-/-}$ vs ID2 DKO	0.0000065
	WT vs $I^{-/-}$	0.0000115
	WT vs $D2^{-/-}$	0.0000308
5A-B	WT vs $D2^{-/-}$ + HU 50 μM	ns
	WT vs $D2^{-/-}$ + HU 100 μM	0.0018921
	WT vs $D2^{-/-}$ + HU 150 μM	0.0019495
	WT vs $D2^{-/-}$ + APH 10 nM	0.0310029
	WT vs $D2^{-/-}$ + APH 25 nM	0.0204921
	WT vs $D2^{-/-}$ + APH 50 nM	0.0004985
	WT vs $I^{-/-}$ + HU 50 μM	ns
	WT vs $I^{-/-}$ + HU 100 μM	ns
	WT vs $I^{-/-}$ + HU 150 μM	ns
	WT vs $I^{-/-}$ + APH 10 nM	ns
	WT vs $I^{-/-}$ + APH 25 nM	ns
	WT vs $I^{-/-}$ + APH 50 nM	0.0120932
	WT vs ID2 DKO + HU 50 μM	ns
	WT vs ID2 DKO + HU 100 μM	ns
	WT vs ID2 DKO + HU 150 μM	ns
	WT vs ID2 DKO + APH 10 nM	ns
	WT vs ID2 DKO + APH 25 nM	ns
	WT vs ID2 DKO + APH 50 nM	ns
5F	WT + HU vs $D2^{-/-}$ + HU	0.00021854
	WT + HU vs $I^{-/-}$ + HU	0.00040459
	WT + HU vs ID2 DKO + HU	0.00062153
5G	WT vs WT + HU	0.000731473
	$D2^{-/-}$ vs $D2^{-/-}$+ HU	0.00065732
	$I^{-/-}$ vs $I^{-/-}$ + HU	0.000321296
	ID2 DKO vs ID2 DKO + HU	0.0001602
6B	WT + APH vs $D2^{-/-}$ + APH	0.000595
	WT + APH vs $I^{-/-}$ + APH	0.009439
	WT + APH vs ID2 DKO + APH	0.000594
	$D2^{-/-}$ + APH vs $I^{-/-}$ + APH	0.001009
	$D2^{-/-}$ + APH vs ID2 DKO + APH	0.011695
6C	WT + APH vs $D2^{-/-}$ + APH	0.002453
	WT + APH vs $I^{-/-}$ + APH	0.014428
	WT + APH vs ID2 DKO + APH	0.003668
	$D2^{-/-}$ + APH vs $I^{-/-}$ + APH	0.013982
6E	WT + HU vs $D2^{-/-}$ + HU	0.004277

Figure	samples	p-value (two tales)
6E	WT + HU vs $I^{-/-}$ + HU	0.015219
	WT + HU vs ID2 DKO + HU	0.00449912
7C	WT + HU vs $D2^{-/-}$ + HU	0.0002692
	WT + HU vs $I^{-/-}$ + HU	0.0195361
	WT + HU vs $I^{-/-}$ (2)+ HU	ns
	WT + HU vs $I^{-/-}$ (12)+ HU	ns
8A	WT vs $I^{-/-}$	0.0240309
	WT vs ID2 DKO	0.012311962
	$D2^{-/-}$ vs $I^{-/-}$	9.91012E-06
	$D2^{-/-}$ vs ID2 DKO	0.00055944
8B	WT vs $D2^{-/-}$ + RS-1	0.00020194
	WT vs $I^{-/-}$ + RS-1	ns
	WT vs ID2 DKO + RS-1	ns
	$D2^{-/-}$ vs $I^{-/-}$	0.01322908
	$D2^{-/-}$ vs ID2 DKO	0.01258901
	$D2^{-/-}$ vs $D2^{-/-}$ + RS-1	1.8008E-09
	$I^{-/-}$ vs $I^{-/-}$ + RS-1	0.000040968
	ID2 DKO vs ID2 DKO + RS-1	0.00031077
S3A-B	WT vs $D2^{-/-}$ + HU 50 μM	ns
	WT vs $D2^{-/-}$ + HU 100 μM	ns
	WT vs $D2^{-/-}$ + HU 150 μM	0.013007
	WT vs $D2^{-/-}$ + APH 10 nM	0.025805
	WT vs $D2^{-/-}$ + APH 25 nM	0.022563
	WT vs $D2^{-/-}$ + APH 50 nM	0.001225
	WT vs $I^{-/-}$ + HU 50 μM	ns
	WT vs $I^{-/-}$ + HU 100 μM	ns
	WT vs $I^{-/-}$ + HU 150 μM	ns
	WT vs $I^{-/-}$ + APH 10 nM	ns
	WT vs $I^{-/-}$ + APH 25 nM	ns
	WT vs $I^{-/-}$ + APH 50 nM	ns
	WT vs ID2 DKO + HU 50 μM	ns
	WT vs ID2 DKO + HU 100 μM	ns
	WT vs ID2 DKO + HU 150 μM	ns
	WT vs ID2 DKO + APH 10 nM	ns
	WT vs ID2 DKO + APH 25 nM	ns
	WT vs ID2 DKO + APH 50 nM	0.0293818
S6	PD20+D2 vs PD20+D2 + HU	0.00052779
	PD20 vs PD20 + HU	0.00204948

Figure	samples	p-value (two tales)
S8	WT vs D2$^{-/-}$	0.001209
	WT vs I$^{-/-}$	ns
	WT vs ID2 DKO	0.012742

Supplementary Figure S1

(A) Schematic of the CRISPR/Cas9-mediated gene targeting to knockout *FANCD2* in WT cells to create D2$^{-/-}$ clone #29. A guide RNA was designed targeting *FANCD2* exon 11 with the Cas9 cut site overlapping with an endogenous BpuEI restriction enzyme recognition site. Indels introduced at the Cas9 cut site (red arrow) would disrupt the BpuEI cut site. Sequence confirmation of biallelic frameshift inducing mutations. (B) Schematic of the CRISPR/Cas9-mediated gene targeting to knockout *FANCI* in D2$^{-/-}$ clone #29 cells to create ID2$^{-/-}$ clone #3. A guide RNA was designed targeting *FANCI* exon 9 with the Cas9 cut site overlapping with an endogenous AcuI restriction enzyme recognition site. Indels introduced at the Cas9 cut site (red arrow) would disrupt the AcuI recognition sequence. Bottom: Sequence confirmation of biallelic frameshift-inducing mutations. (C) Schematic of the CRISPR/Cas9-mediated gene targeting to knockout *FANCI* in D2$^{-/-}$ clone #39 cells to create the ID2$^{-/-}$ DKO clone #4. A guide RNA was designed targeting *FANCI* exon 9 with the Cas9 cut site overlapping with an endogenous AcuI restriction enzyme recognition site. Indels introduced at the Cas9 cut site (red arrow) would disrupt the AcuI recognition sequence. Sequence confirmation of biallelic frameshift inducing mutations. (D-E) *D2*$^{-/-}$, *I*$^{-/-}$ and *ID2* DKO cells do not express truncated forms of FANCD2 or FANCI. (D) WCEs from WT, *D2*$^{-/-}$ (clone #39, exon 12 deletion), and ID2 DKO (clone #1) cells were analyzed for the presence of full length FANCD2 (166 kDa) and truncated FANCD2 (expected size of truncated FANCD2 expressed from exons 1-11: 35.8 kDa) via western blot and whole membrane analysis using an antibody that recognizes the N-terminus of FANCD2 (Santa Cruz; sc-20022, 1:1000). Tubulin was used as a loading control. (E) WCEs from WT, *I*$^{-/-}$ (clone 28, exon 10 deletion), and ID2 DKO (clone #1) cells were analyzed for the presence of full length FANCI (146 kDa) and truncated FANCI protein

(expected size of truncated FANCI expressed from exons 1-9: 27.9 kDa) via western blot and whole membrane analysis using an antibody that recognizes the N-terminus of FANCI (Bethyl; A300-212, 1: 1000). *Note*: Samples were run only briefly on an 8-16% gradient gel to allow detection of small protein sizes. On these gels, a non-specific band appears to co-migrate with full length FANCI, however, longer sample runs on low % gradient gels reveal that there is no detectable full length FANCI protein in *I*$^{-/-}$ and *ID2* DKO cells (Figure 3A, B).

Supplementary Figure S2

FANCD2 and FANCI act in concert to activate the MMC-triggered intra-S phase checkpoint. WT, *D2*$^{-/-}$(clones #29 and #39), *I*$^{-/-}$ (clones #28 and #30) and *ID2* DKO (clones #1 and #2) cells, as well as the complemented counterparts, were untreated or treated with 10 nM MMC for 20 hr, followed by propidium iodide (PI) staining and FACS analysis. Shown is a graphic representation of the average percentage of the indicated cell populations present in the G1, S and G2/M phases of the cell cycle. Average percentages were determined from a minimum of 3 replicates and data points were averaged between clones of identical genetic backgrounds.

Supplementary Figure S3

(A) FANCD2, but not FANCI, promotes cellular resistance to HU. WT, *D2*$^{-/-}$(clone #29), *I*$^{-/-}$ (clone #30) and *ID2* DKO (clone #2) cells were plated at low density and incubated with increasing doses of HU (0 to 150 μM) for 12 to 14 days to allow for single cell colony formation. Plates were fixed and stained with Coomassie, and colonies with a minimum of 50 cells were scored. Results were averaged from a minimum of 3 replicates and normalized to the respective untreated cells. Error bars represent the standard deviation and significance was determined by t-test. Statistical significance at $p < 0.05$, $p < 0.01$, and $p < 0.001$ are indicated as *, **, ***, respectively. (B) FANCD2, but not FANCI, promotes cellular resistance to

APH. WT, *D2*$^{-/-}$(clone #29), *I*$^{-/-}$ (clone #30) and *ID2* DKO (clone #2) cells were plated at low density and incubated with increasing doses of APH (0 to 50 nM) for 12 to 14 days to allow for single cell colony formation. Plates were fixed and stained with Coomassie, and colonies with a minimum of 50 cells were scored. Results were averaged from a minimum of 3 replicates and normalized to the respective untreated cells. Error bars represent the standard deviation and significance was determined by t-test. Statistical significance at $p < 0.05$, $p < 0.01$, and $p < 0.001$ are indicated as *, **, ***, respectively.

Supplementary Figure S4

FANCD2 and FANCI cooperate to promote CtIP foci formation following replication stress. WT, *D2*$^{-/-}$ (clone #39), *I*$^{-/-}$ (clone #28) and *ID2* DKO (clone #1) cells were untreated or treated with 2 mM HU for 20 hr. Nuclear CtIP foci formation was analyzed by fluorescence microscopy and representative images were taken. Nuclei with >5 foci were considered positive for CtIP foci formation.

Supplementary Figure S5

FANCD2 and FANCI are dispensable for RAD51 foci formation during replication stress. WT, *D2*$^{-/-}$ (clone #39), *I*$^{-/-}$ (clone #28) and *ID2* DKO (clone #1) cells were untreated or treated with 2 mM HU for 20 hr. Nuclear RAD51 foci formation was analyzed by fluorescence microscopy and representative images were taken. Nuclei with >5 foci were considered positive for RAD51 foci formation.

Supplementary Figure S6

FANCD2 is dispensable for replication stress-induced RAD51 foci formation in a human fibroblast cell line. An FA-D2 patient-derived cell line (PD20) and its complemented

counterpart (PD20+D2) were untreated or treated with 2mM HU for 20 h. Cellular nuclei were analyzed for the presence of RAD51 foci. Nuclei with >5 foci were considered positive for RAD51 foci formation.

Supplementary Figure S7

FANCD2, but not FANCI, functions to promote ANHEJ-mediated DNA DSB repair. WT, *D2*$^{-/-}$(clone #39), *I*$^{-/-}$ (clone #28) and *ID2* DKO (clone #1) cells, as well as the complemented counterparts, were used for this analysis. In this assay, I-Scel digestion creates a DSB in the ANHEJ reporter plasmid (EJ2-GFP). Repair of the DSB by microhomology-mediated repair restores GFP expression. The repair percentage was determined by the number of dual GFP and mCherry positive cells divided by the number of mCherry positive cells (transfection control). Results were averaged from a minimum of 3 replicates. Error bars represent the standard deviation and significance was determined by t-test. Statistical significance at $P<0.05$, $P<0.01$, $P<0.001$, $P<0.0001$ are indicated as *, **, ***, **** respectively.

Supplementary Table 1

List of primer sequences used during Golden Gate Cloning and for the confirmation of correctly targeted FANCD2 and FANCI exon sizes and sequences.

Supplementary Table 2

Summary of all P-values for results shown in Main Figures 4 to 8, and in Supplementary Figures S3, S6 and S8.